Received: 10 July 2024 | Revised: 1 November 2024 | Accepted: 16 December 2024

High Voltage

DOI: 10.1049/hve2.70042

国家电网 STATE GRID 中国电力科学研究院有限公司 CHINA ELECTRIC POWER RESEARCH INSTITUTE | The Institution of Engineering and Technology | WILEY

ORIGINAL RESEARCH

Analysis of micro-discharges fine dynamics via x-ray detection on the high voltage Padova test facility experiment

Federico Caruggi[1,2] | Gabriele Croci[1,2,3] | Stephanie Cancelli[1,2,3] | Agostino Celora[1] | Antonio De Lorenzi[4] | Michele Fincato[4] | Giuseppe Gorini[1,2,3] | Giovanni Grosso[3] | Federico Guiotto[5,6] | Enzo Lazzaro[3] | Luca Lotto[7] | Nicola Pilan[5] | Oscar Putignano[3] | Silvia Spagnolo[4,5] | Marco Tardocchi[1,3] | Andrea Muraro[2,3]

[1]Department of Physics "G. Occhialini", University of Milano-Bicocca, Milan, Italy

[2]INFN, Sezione Milano-Bicocca, Milan, Italy

[3]Istituto per la Scienza e Tecnologia dei Plasmi, CNR-ISTP, Milan, Italy

[4]Istituto per la Scienza e Tecnologia dei Plasmi, CNR-ISTP, Padova, Italy

[5]Consorzio RFX (CNR, ENEA, INFN, Università di Padova, Acciaierie Venete SpA), Padova, Italy

[6]Centro Ricerche Fusione (CRF) - University of Padova, Padova, Italy

[7]Dipartimento di Ingegneria Industriale – DII, Università di Padova, Padova, Italy

Correspondence
Federico Caruggi.
Email: f.caruggi@campus.unimib.it

Associate Editor: Zhiyuan Liu

Funding information
EUROfusion, Grant/Award Number: 101052200

Abstract

The high voltage Padova test facility (HVPTF) is an experiment set in Padova, Italy, operating in the framework of the Neutral Beam Test Facility project of the International Thermonuclear Experimental Reactor (ITER). One of the purposes of HVPTF is to study the phenomenology of discharge events occurring between electrodes at high voltage differences over long vacuum gaps, which is crucial in the development of the neutral beam injector foreseen for ITER. The facility hosts a cylindrical vacuum vessel with stable pressure control, where two electrodes of different possible geometries can be mounted. Two independent power supplies allow for total voltage differences up to 800 kV_{DC} with adjustable gap widths up to 250 mm. Among the diagnostics, a gas electron multiplier (GEM) detector is installed for acquisition of x-ray emission on a radial line of sight of the vessel. This paper presents a study of the experimental sessions featuring stainless-steel needle-plane electrodes. The analysis is based on the GEM data, in relation to the information on current and voltage of the two power supplies. The events are characterised in terms of both temporal and spatial evolution, providing sequential emission profiles with spatial resolution of tens of millimetres on timescales of the order of hundreds of nanoseconds.

1 | INTRODUCTION

In the framework of the research for nuclear fusion power production, the International Thermonuclear Experimental Reactor (ITER) is under construction in Cadarache, France. The aim for this device is to demonstrate the feasibility of energy production through magnetically confined nuclear fusion reactions with a Q-value of 10. Among the external heating systems needed by the plasma, the use of neutral beam injectors (NBI) is foreseen. The device is designed to perform acceleration of a negative ion beam with a current of 40 A up to energies of 1 MeV, followed by its neutralisation and direct

injection in the plasma, where energy can be transferred through collisions. ITER requires two NBIs, each one to deliver 16.7 MW power for up to 3600 s [1].

In the context of the Neutral Beam Test Facility, the programme responsible for the research and development of the NBI, the megavolt ITER injector concept advancement (MITICA) experiment is under commissioning in Padova, Italy [2]. It consists of a full-scale prototype of the NBI, featuring the use of five accelerating grids in vacuum (each gap with 200 kV voltage difference) to obtain the high beam energies required. A representation of the device is displayed in Figure 1.

One of the major challenges in its operation is thus high voltage holding capabilities over long vacuum gaps. The main issue in this context is the occurrence of electrical discharges, phenomena observable as spikes of current concurrent with voltage drops that can prevent the system correct operation. In this work, discharges are classified either as micro-discharges, which are those from which the system can recover autonomously, or breakdowns, more violent occurrences where the system fully switches off, and manual intervention is needed to restore operation. Events of the latter kind can cause serious damage to the equipment as well. The study of micro-discharges and breakdown precursors can be of help in the design of a control system for breakdown prevention and safe operation of the MITICA accelerator.

In order to gain a better understanding of the phenomenology of discharges, the high voltage Padova test facility (HVPTF) experiment has been set up in support of MITICA operations [3]. It consists of a large vacuum vessel (about 2.4 m^3) in which two electrodes are mounted. Electrodes of various shapes can be used to study different configurations, and their distance can be varied up to 250 mm. Two independent power supplies provide voltage differences up to 800 kV_{DC} with the possibility to use single or double polarity. Current and voltage of both power supplies are monitored with a sampling frequency of 100 Hz together with the pressure inside the chamber (measured by different instruments located in multiple positions around the wall of the vacuum vessel). Additional diagnostics feature a residual gas analyser for the composition of the gas mixture going out of the chamber and multiple cameras for various light spectrum regions and with various sampling rates. During operation, the vessel is also characterised by emission of x-rays, mainly produced by Bremsstrahlung radiation of the electrons extracted and accelerated in the discharges. These are monitored as well, with the combined use of inorganic scintillators and, since 2022, gas electron multiplier (GEM)-based detectors. A picture of the rear of the HVPTF vessel with the scintillators is shown in Figure 2. Correlations between the dynamics of the power supply currents and the x-rays have been observed in the past already [4, 5]. Because of the higher speed of the signal, a more detailed analysis of the emitted radiation can be of help in the search for breakdown precursors, and real-time analysis of the emission profiles can possibly aid in the design of a feedback-loop control system for the experiment with the aim of granting safe operative conditions in the context of the MITICA experiment and the ITER NBI as well.

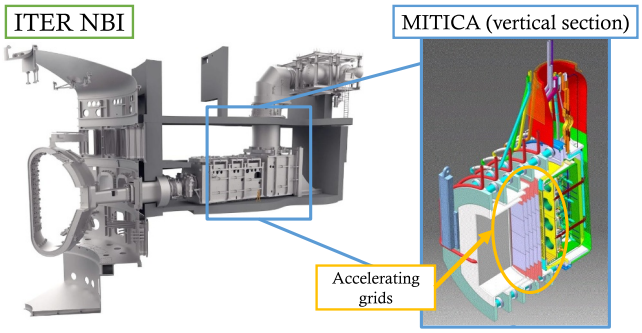

FIGURE 1 View of a 3D rendering of the ITER NBI and section of MITICA. ITER NBI, International Thermonuclear Experimental Reactor neutral beam injector and MITICA, megavolt ITER injector concept advancement.

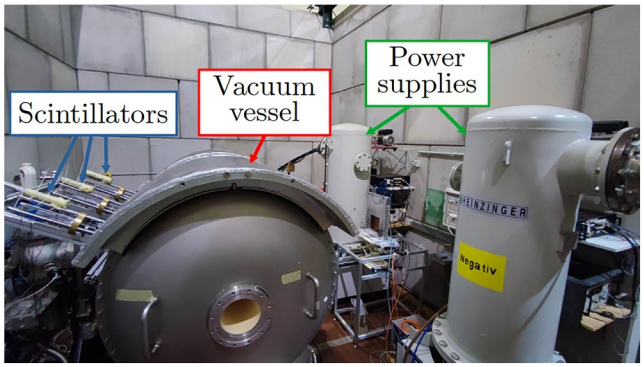

FIGURE 2 Picture of the high voltage Padova test facility vacuum vessel and setup.

2 | GEM DETECTORS

A GEM foil [6] is a thin sheet of kapton (50 μm thick), with both sides covered by a layer of metal coating (commonly Cu, 5 μm thick but Al can be the choice as well [7]), in which a series of micro-holes is etched with a high density pattern. The application of a voltage difference between the two metal faces produces high dipole fields in the holes. This property can be exploited for electron multiplication and signal amplification.

A GEM detector is a gaseous detector in which the signal is generated by the gas ionisation in the drift region of the active volume caused by the incoming radiation (x-rays in this case). The extracted electrons are accelerated towards the foils by the electric field and are multiplied as they traverse the holes. Multiple foils in cascade are commonly employed in order to achieve high gain levels without having to apply too high voltage differences across a single foil. The signal is collected by a pixelated anode at the end, providing information about the spatial distribution of the incoming radiation. A schematic representation of the detector is shown in Figure 3, referencing three GEM foils which delimit four volumetric regions, and the different values of voltage imposed on each channel of the HV module. The detector employed in this work consists of a

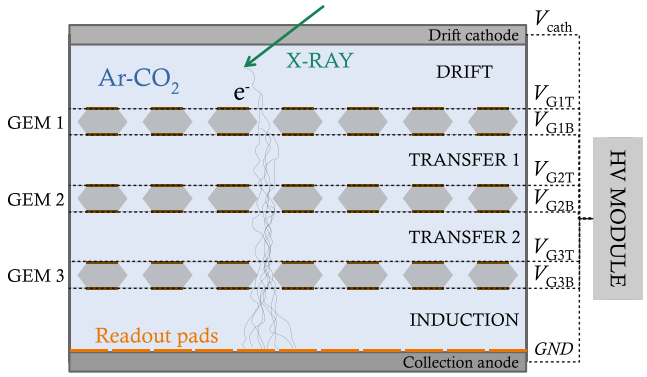

FIGURE 3 Schematic representation of a triple GEM detector. GEM, gas electron multiplier.

stack of three foils metal-coated with Cu. It contains a mixture of Ar-CO_2 70%–30% and the collection anode is composed by 256 pads, 6 × 6 mm^2 each with a total active area of 100 cm^2.

The detector is coupled with a digital readout chain made by the combination of custom-made application-specific integrated circuits (ASICs) named GEM integrated interface (GEMINI) [8] and field programmable gate arrays, able to record, for each event, the timestamp, the incidence position on the anode (each pixel, or pad, correspond to one channel) and some information about energy through the use of the time-over-threshold measurement (more details can be found in Muraro et al. and Cancelli et al. [9, 10]). The detector can be thus used for fast and accurate single photon counting. The system features both great temporal resolution (< 1 ms) and good spatial resolution (in the order of few mms), together with a decent energy resolution (20% at 6 keV).

GEM-based detectors are especially useful for charged particle tracking and x-ray detection, for various applications [11, 12], but with the use of suitable converters they can also be adapted for fast or thermal neutron detection [13–15].

It must be mentioned that unfortunately one of the ASICs connected to the detector was damaged during the experimental runs, thus the images of the spatial distribution of the radiation reported in the following sections have always one-quarter (the top left one) void of counts.

2.1 | Data clusterisation

In common practice, the analysis of data collected from a pixelated anode, as the one used in the GEM detector, foresees a process called clusterisation. The passage of a single photon in the active volume produces generally more than one electron, so that multiple channels collect charge for the same event. The clusterisation process consists in the aggregation of the signals of the single pads, depending on timestamps and position, to reduce them to a single event corresponding to the photon with its total deposited charge. A first analysis of the data collected in this work, however, showed signs that the detector reached counting saturation during the discharges, so that it got paralysed (meaning that it lost some events) or, more probably, it reached the conditions of pile-up on the events (meaning that multiple events are recorded as a single one). Because of this, the analyses presented in the following were performed without clusterisation of the data, meaning that for each time a pixel collected charge, a separate event was recorded. The intensity of the x-ray signal in the time traces of this text will thus be represented as arbitrary units instead of number of incoming x-rays. The pile-up issue can additionally cause overflow of the time-over-threshold measurements, so that the information cannot be converted accurately to charge and energy values. For this reason, in the following analyses, the radiation spectra were not taken into account.

3 | DATA COLLECTION AND ANALYSIS

During the experimental sessions considered, the detector was installed on a radial line of sight of the HVPTF vacuum vessel, behind a Beryllium window which allows passage of the x-rays. The flange has a support for a Pb collimator to be mounted in order to reduce the incoming flux of particles on the detector but for the data collected for this work the full flange width was used (13 mm diameter). A schematic of the configuration is displayed in Figure 4, and a picture of the setup in Figure 5. Moveable components (represented in the scheme by the double dashed grey arrows) of the GEM support allowed for a variation of the range of view, depending on the distance between the detector and the collimator (the further away the detector is placed, the more restricted is the view range and the more magnified the objects are seen).

A stainless steel needle, 29 mm long, was used as cathode, whereas the anode was a plane of 108 mm diameter, also made of stainless steel. The distance between the electrodes was fixed at 36 mm. A picture of the electrodes mounted inside the chamber is shown in Figure 6. During the experimental sessions examined, single polarity was used, which means that the cathode was brought at negative voltages and the anode was kept at ground.

The experimental procedure consisted in the application of successive voltage steps in order to achieve what is called electrode conditioning, which refers to the development of the capabilities of the electrodes themselves to sustain high voltage differences without breakdowns (a more detailed description of the process can be found in Pilan et al. [16]). In this instance, the GEM detector was able to observe the emission of Bremsstrahlung x-ray radiation produced by the electrons extracted during the discharges and impinging on solid obstacles, giving information about the dynamics of the phenomena. A needle was chosen as cathode in order to have more favourable conditions for electron extraction (because of the strongly divergent electric field), hence the occurrence of micro-discharges, mainly with the aim of obtaining large datasets in relatively short time for extensive analyses. Examples of additional results obtained for the same experimental sessions, not mentioned in this work, were presented in Caruggi et al. [17]. All the studies described here were performed with the use of a custom data analysis software developed by

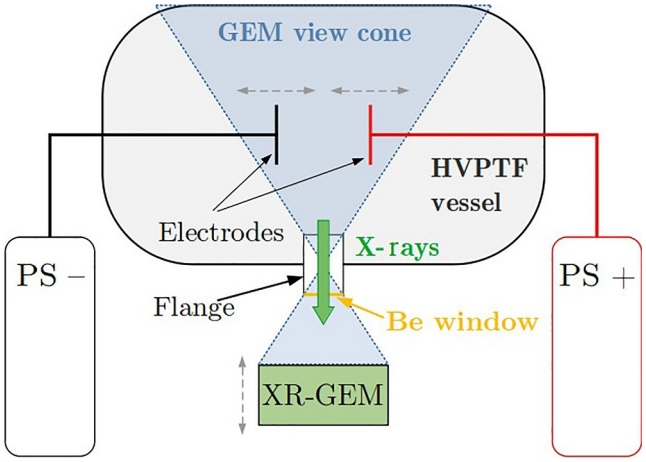

FIGURE 4 Schematic representation of the GEM detector setup on HVPTF. GEM, gas electron multiplier and HVPTF, high voltage Padova test facility.

FIGURE 5 Picture of the gas electron multiplier detector installation.

the authors, tailored for the display of GEM detector data and for the comparison with the analogue signals of HVPTF.

3.1 | Time traces

The first analysis was performed on the temporal evolution of the x-ray emission collected by the detector with reference to

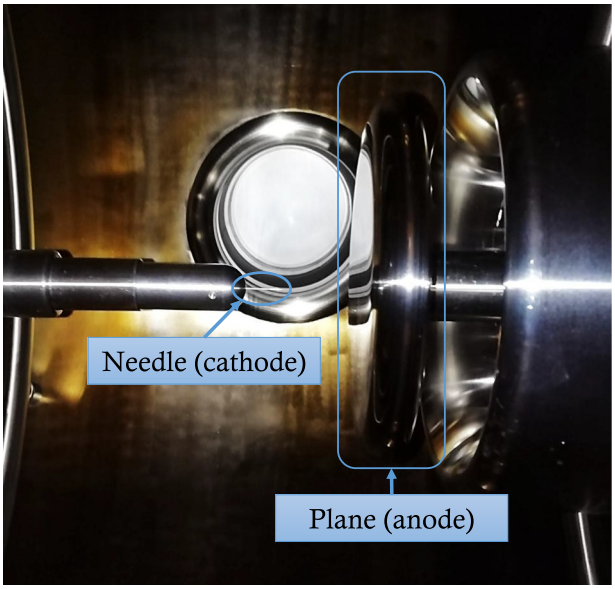

FIGURE 6 Picture of the electrodes inside the high voltage Padova test facility vessel.

the current and voltage signals coming from the analogue readout of the power supplies. A first view of a full conditioning ramp is displayed in Figure 7a, displaying current, pressure, voltage and x-ray signals. As can be seen, at the beginning of the steps the x-ray emission is absent, and it starts to be detected after reaching a high enough value of voltage on the negative electrode, approximately 120 kV. Following that, a continuous background of counts is recorded by the detector, interspersed with signal spikes, occurring in correspondence of spikes in the current signal and drops of voltage. These are the micro-discharges mentioned above, superimposed, for what concerns the x-ray signal, to the continuous dark current emission developing between the electrodes (i.e. the Fowler–Nordheim emission current), a phenomenon analogous to what is described in Spada et al. [18].

A more detailed view is shown in Figure 7b which better highlights the strong correlation between the analogue and x-ray signals, in the sense that, for each current peak and voltage drop, there is a corresponding structure on the x-ray emission profile (a fact that can be seen here more clearly with respect to the full-ramp picture). As previously mentioned, these correlations were already observed in the past (see e.g. [4, 5]) and they can be justified considering that the majority of the x-rays observed come from Bremsstrahlung radiation of the electrons involved in the discharges.

In the final section of the ramp, the voltage value is kept constant to try and reach stability in the system (ideally the aim is a situation where micro-discharges are absent), and after the last voltage step the breakdown happens, meaning that the voltage drops too much for the system to recover, and the system itself shuts down. From the figures, we can also see that the system experiences an increase of pressure at the end of the conditioning ramp, where the micro-discharges are more frequent. This is possibly caused by gas desorption from

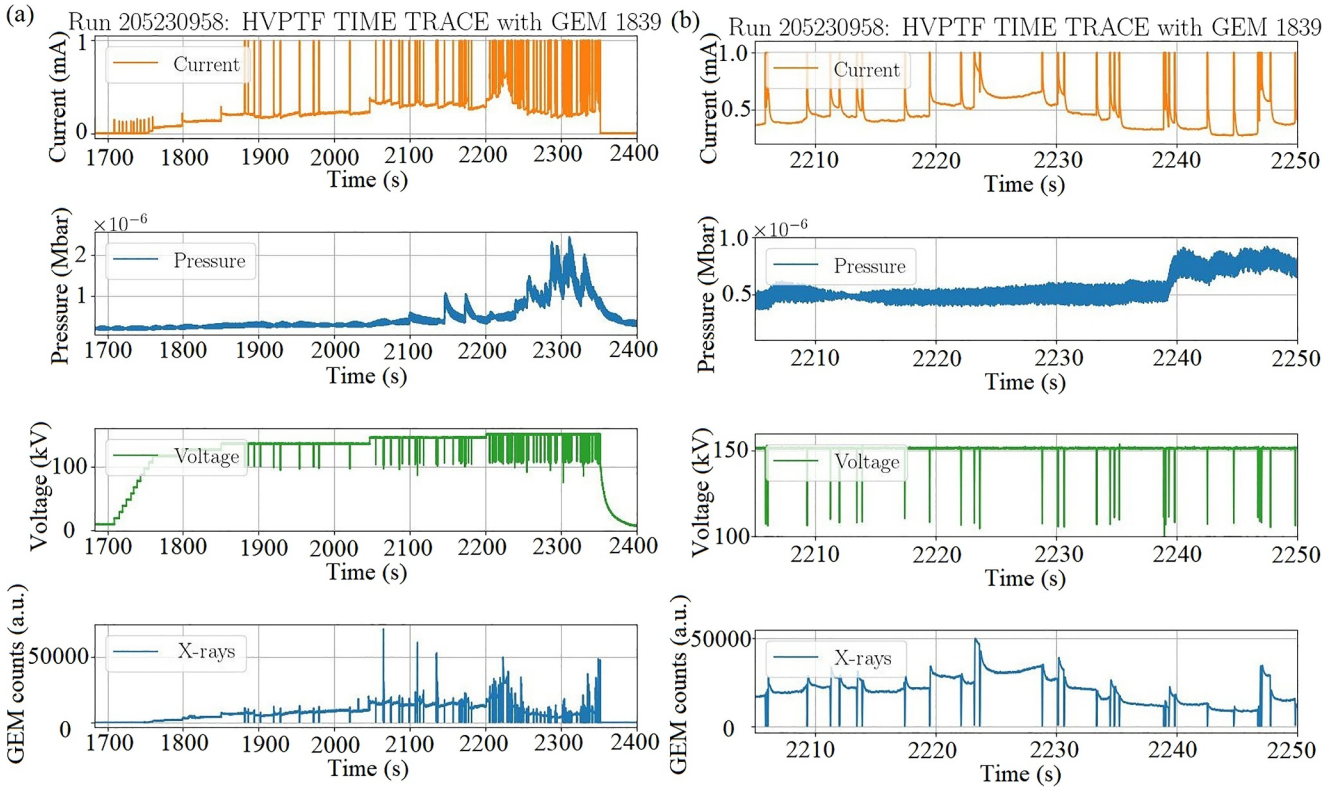

FIGURE 7 Time evolution of analogue and x-ray signals during the experimental session studied. (a) View of the signals during the full 700 s ramp. (b) Zoom of the graph in (a) from 2205 to 2250 s.

the electrode surfaces caused by the discharges themselves [19].

Details on an even smaller timescale are shown in Figure 8, with plots showing current and voltage signals from the analogue system and x-ray signal from the GEM detector, during a single micro-discharge (over a 0.14 s time window).

Firstly, we can see that the micro-discharge, appearing in Figure 7 as a single point spike, has more structure underneath: the current signal shows two rising features, one right after another. Here, it is assumed that the first one corresponds to the micro-discharge spike itself, whereas the other is intrinsically produced by the system, needing to feed current to increase the voltage after its drop. It can be also seen that the analogue system alone is not enough to perform a detailed analysis of the phenomena, because of the limited full scale of the current measurement which caps at 1 mA and the sampling frequency which is quite low (100 Hz). Additionally, the fact that the current is measured at the power supplies implies that the signal is not really representative of what happens between the electrodes, because of the presence of additional elements in the interposed electrical circuit with their own contributions. Because of these issues, it becomes unfeasible to derive meaningful data about the dynamics of the micro-discharge from the analogue measurement alone. Analysis of the x-ray signal plot instead, with a denser binning, shows more features about the emission. The continuous background already

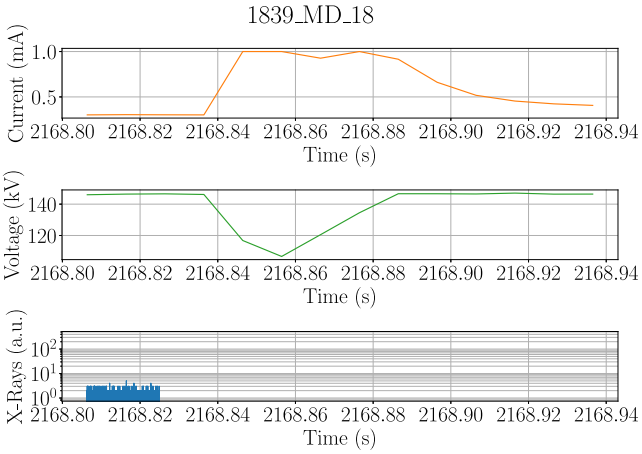

FIGURE 8 Time evolution of x-ray signal in a single micro-discharge with a 0.14 s window.

mentioned before is still present, but we can see that its intensity is much lower in relation to the signal spike during the micro-discharge. The latter appears again as a single short spike, after which the emission switches off until the voltage is brought back up to nominal value. The capability of the GEM detector to measure the spatial distribution of the incoming radiation can be also firstly exploited, as shown in Figure 9, to see that the continuous background (the picture shows the

cumulative events of a 10 s window) comes from a region where we expect to monitor radiation coming directly from the plane anode (a reference schematic is superimposed to show the expected positions of the electrodes in the view range of the GEM detector).

We can exploit the great temporal resolution capabilities of the GEM detector to have much lower sampling times and again look at the dynamics underneath what appears, on larger timescales, as a single spike. Figure 10a shows a plot of the evolution in time of x-ray radiation detected for a single micro-discharge with a sampling time of 100 ns, and new details appear. The plot shows firstly a peak with small intensity, bifurcated, which lasts for about 1 μs. This is followed by some silence (absence of counts of the detector), with a duration of approximately 2 μs, and then the real spike of high intensity. Here the limit of the detector can be seen, since the peak is not a single point but a capped rising feature. The maximum reached is about 400 units, corresponding to 4 Gcps for the digital acquisition chain. After the spike, we can see from the plot a lower intensity plateau, lasting for about 15 μs, followed by again absence of counts. This is the silence caused by the drop in system voltage and has a duration of about 20 ms, orders of magnitude longer with respect to the micro-discharge itself, as seen from the previous plot of Figure 8.

This observed dynamics is heavily consistent across all the micro-discharges analysed, so that the counts per bin can be summed up to have more statistics on the data taken into account. The resulting graph of the cumulative counts in time for a full conditioning ramp is shown in Figure 10b, and it can be seen that all the features just observed are still recognisable with a smoother plotted curve. The consistency was found also across the various conditioning ramps taken into account for this study, even if only a single set of data is presented here in detail for the sake of simplicity. Multiple consecutive conditioning ramps, among which the detector distance was changed, still showed the same dynamics in the time evolution of the signal, with the only difference being in the spatial distribution of the radiation (as mentioned before, with the view range and level of magnification depending on the position of the detector on the supports).

3.2 | Space-time analyses

Following the first analysis, the capabilities of the GEM detector were exploited to perform a combined study of the distribution of events in both space and time, looking at the time dynamics of the signal collected by each channel and grouping together pads with the same evolution. Again, the counts from all the micro-discharges of a conditioning ramp are summed to achieve better statistics. The analysis shows the presence of three of these groups, the characteristic dynamics of which are illustrated in the following. Figure 11a displays the reference time trace with the three regions highlighted in different colours, and Figure 11b shows the reference image of the dark current counts to identify the position of the pads in

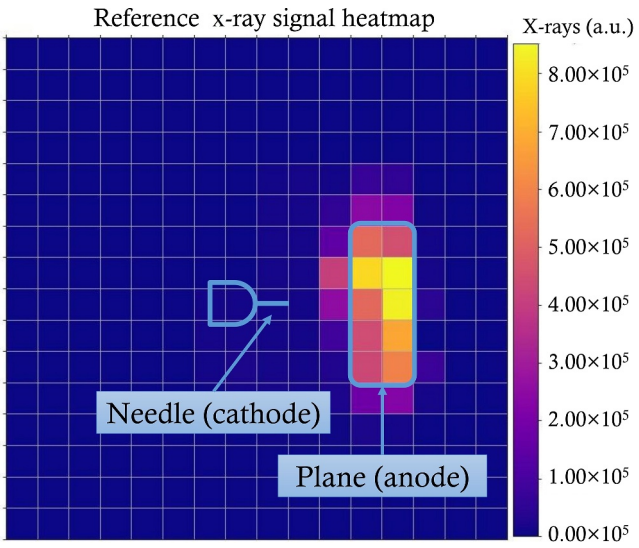

FIGURE 9 Heatmap of the x-ray detected for dark current signal (with a 10 s sampling window), with schematic representation of the expected placement of the electrodes.

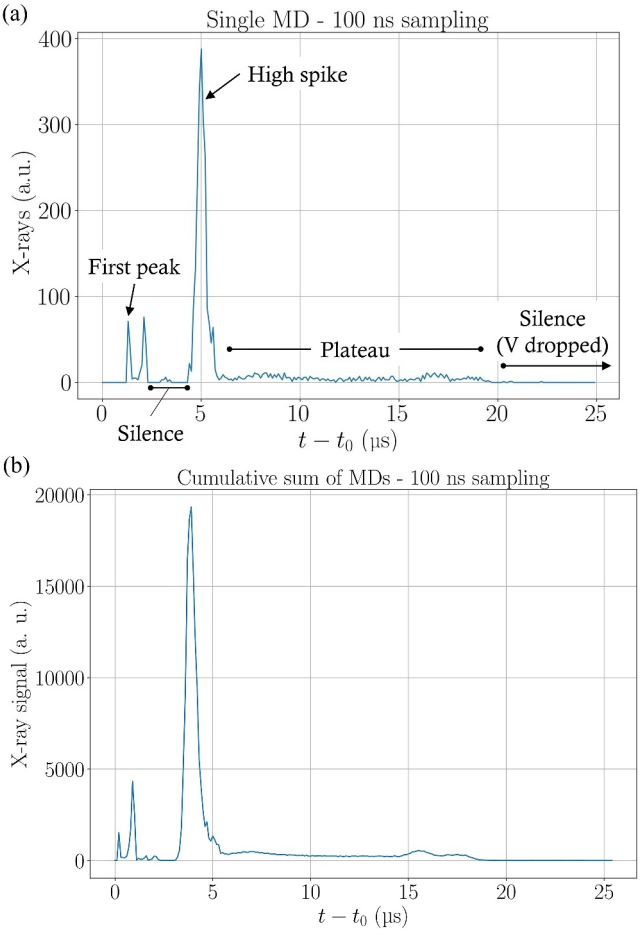

FIGURE 10 Time evolution of x-ray signal in the micro-discharges, with reference to an arbitrary t_0 chosen as start of the discharge itself. (a) Single micro-discharge view. (b) Cumulative signal across all micro-discharges.

the GEM view range, with the same colour code for the groups as the former (the yellow pad group is made of all the pads that have no coloured border).

The pixels that have a line of sight towards the chamber walls (surrounding the space where the electrodes are placed) show signal only during the first 5 μs approximately, contributing only to the first bifurcated peak and the full spike (Figure 12a). The pixels looking at the plane electrode instead, which are the ones detecting the continuous background of counts (dark current signal) during the whole run, exhibit no signal during the spikes, and they have counts only after the 5 μs mark. The apparent plateau of the previous subsection is shown instead as a gradual descent (Figure 12b), pertaining only to some pads that have a line of view of the space immediately around the plane. Two final increments of counts can be seen on the time trace of the pixels looking directly at the centre of the plane electrode (Figure 12c).

The consistency of the time dynamics across all the micro-discharges mentioned before also allows to have enough statistics to produce the images of the single frames corresponding to the cumulative time dynamics plot. The reference time trace is shown once again in Figure 13, with regions highlighted similarly to the previous analysis. In this case, there are four distinct colours as the first bifurcated spike shows a different dynamics with respect to the high peak. Figures 14–17 show the sequences of frames for the different regions of the time trace, calculated for the time values

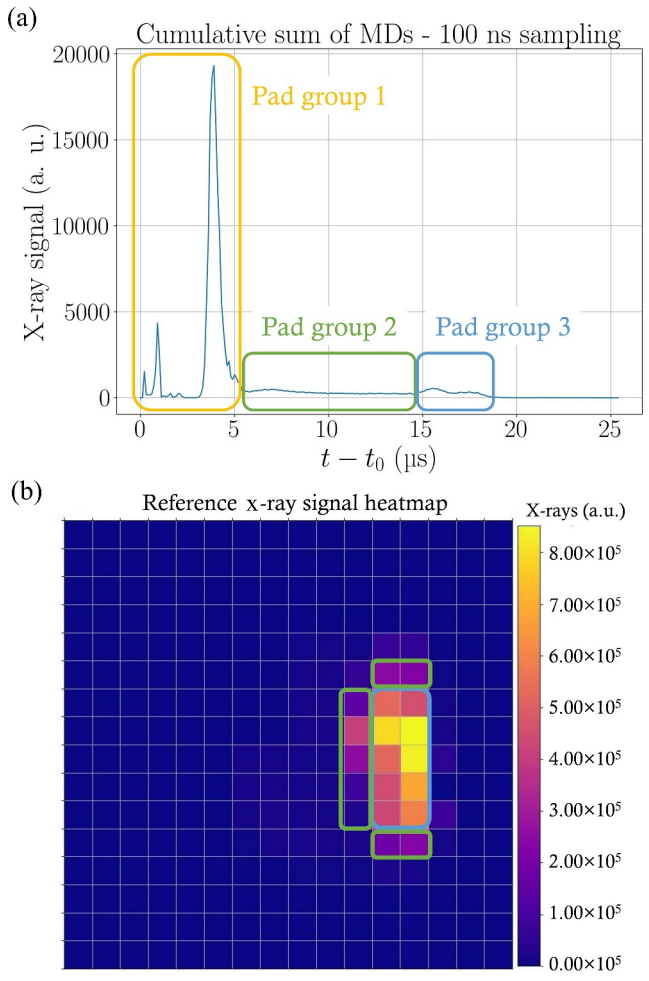

FIGURE 11 Space-time analysis of the micro-discharges. (a) Reference time evolution of all micro-discharges. (b) Heatmap of incoming radiation, with the groups distinguishable by colours.

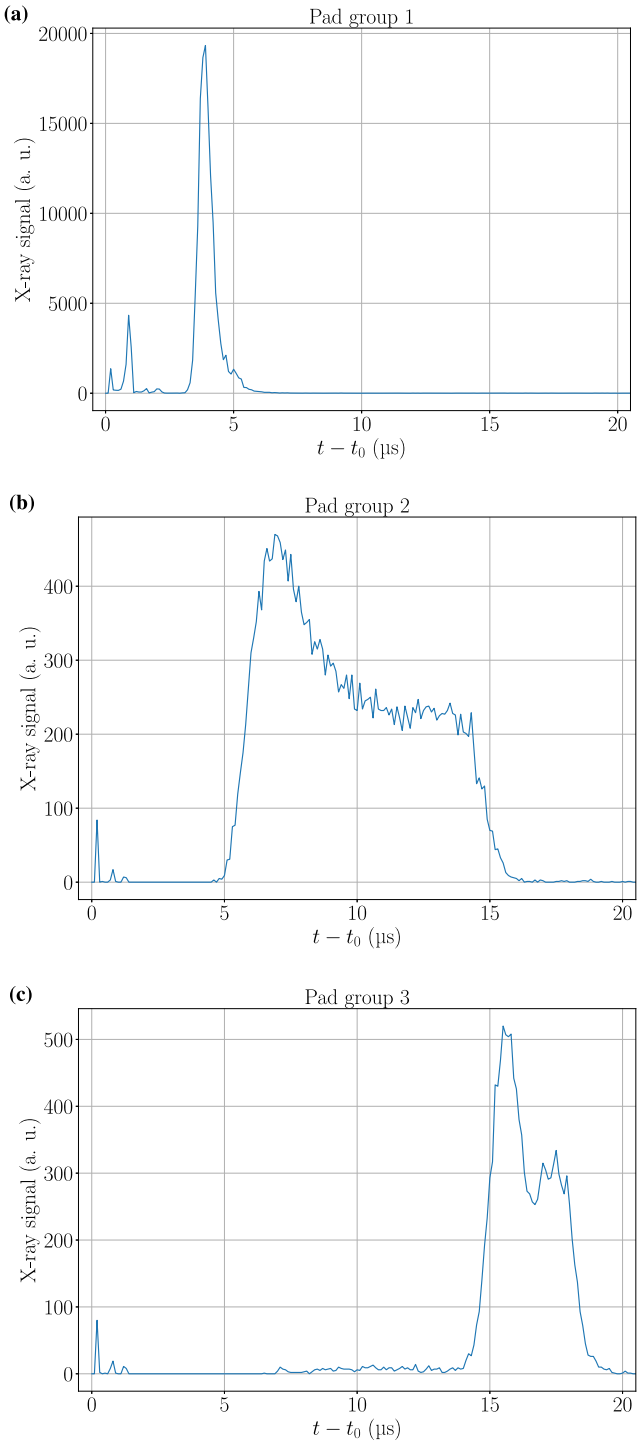

FIGURE 12 Time evolution of x-ray signal for the three pad groups for the cumulative micro-discharges. (a) Chamber pads. (b) Around-plane pads. (c) Centre-plane pads.

indicated by the dashed lines in the main picture, and with borders of the corresponding colour. In particular, Figure 14, corresponding to the bifurcated spike, shows that the emission of x-rays, initially located around the anode, diverges outward to the edges of the detector view range. This phenomenon can be interpreted as the fact that the electrons which emit Bremsstrahlung radiation are deviated from their path towards the anode to go towards the chamber walls and surroundings.

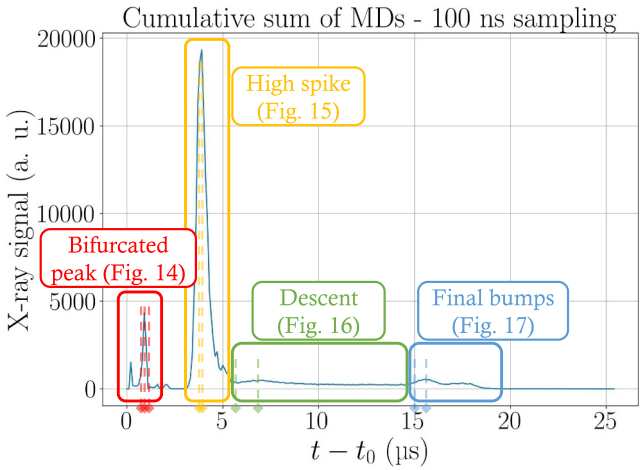

FIGURE 13 Reference time evolution of all micro-discharges with the four groups distinguishable by colours, and reference to Figures 14–17. Dashed lines with arrows correspond to the temporal marks of the frames selected for the heatmaps.

This is observed twice, in correspondence to the two bifurcations of the spike. Figure 15, taken from frames in the high peak, shows contribution to the signal from all the pixels except for those looking at the plane electrode. During the descent, as mentioned before and as shown in Figure 16, only the pads with lines of sight around the plane have counts, as if the electrons were hitting a different larger surface around it. After the 15 µs mark, as presented in Figure 17, the radiation is back on the pixels receiving signals from the central part of the plane, as is the case of the dark current signal, just before the micro-discharge is over with the event counts dropping to zero.

3.3 | Considerations

The dynamics of the micro-discharges that were observed and presented above can suggest a combination of the effects, for example, of virtual anode and plasma sheath. The dynamics of the electron trajectories can be inferred from the Bremsstrahlung x-ray emission profiles as previously mentioned. From the GEM-collected data we can thus deduce that, at the beginning of the micro-discharges, electrons that normally are going towards the anode are deviated on their path towards the chamber walls. This, as previously mentioned, can be the effect of a local modification of the voltage around the plane electrode (see Figure 14). It is worth pointing out that, as already stated, the experimental session was performed in single

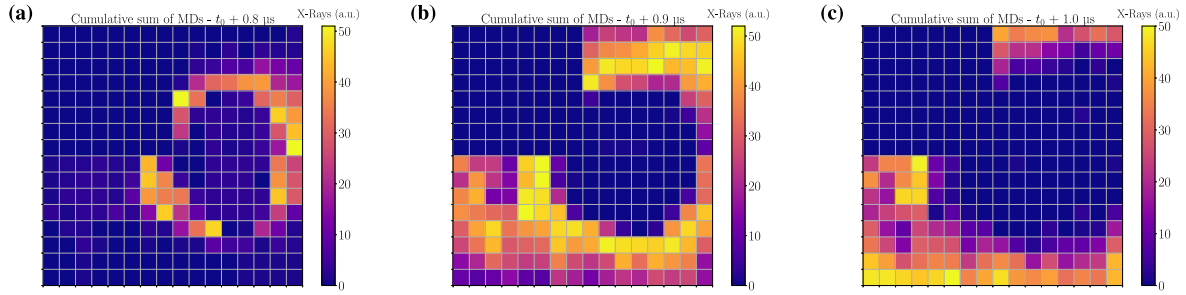

FIGURE 14 Evolution of the spatial distribution of the detected radiation during the bifurcated peak of the micro-discharge. (a) Frame taken at 0.8 µs. (b) Frame taken at 0.9 µs. (c) Frame taken at 1 µs.

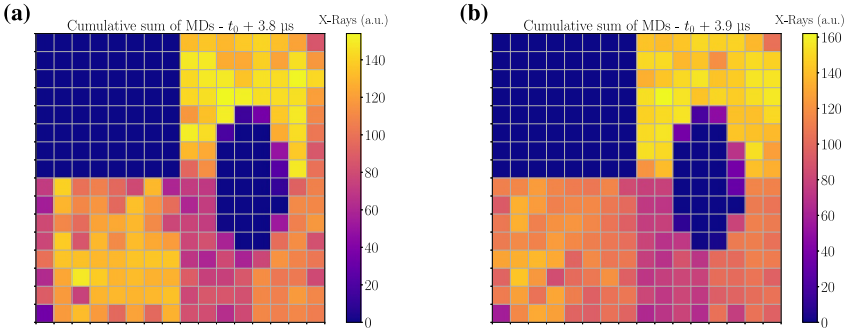

FIGURE 15 Evolution of the spatial distribution of the detected radiation during the high spike of the micro-discharge. (a) Frame taken at 3.8 µs. (b) Frame taken at 3.9 µs.

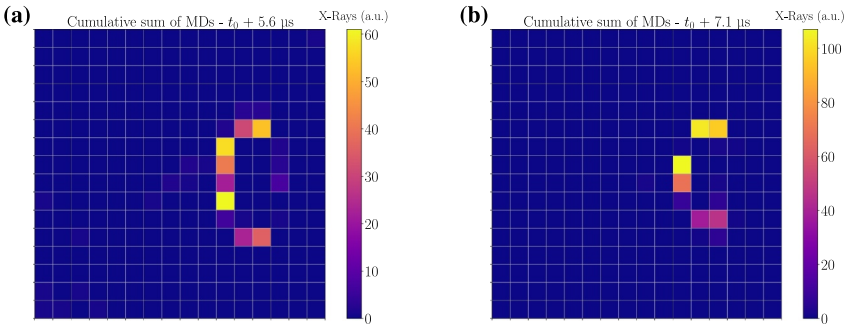

FIGURE 16 Evolution of the spatial distribution of the detected radiation during the descent of the micro-discharge. (a) Frame taken at 5.6 µs. (b) Frame taken at 7.1 µs.

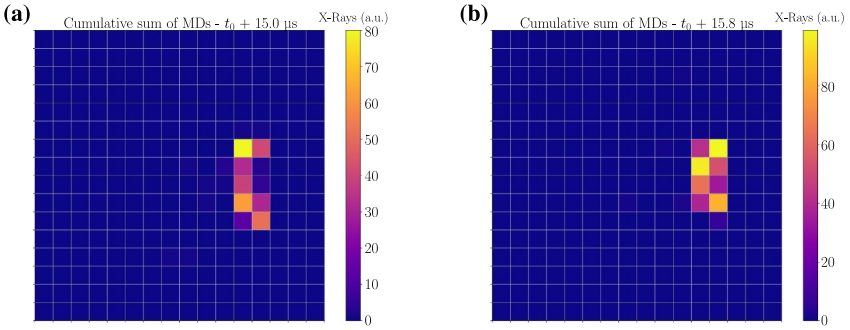

FIGURE 17 Evolution of the spatial distribution of the detected radiation during the final bumps of the micro-discharge. (a) Frame taken at 15 µs. (b) Frame taken at 15.8 µs.

polarity, so that the anode was kept at ground, the same potential level of the surrounding structures in the chambers (walls and electrode supports). This could imply that the variation of local electric field around the plane electrode needed to achieve the deviation effect is not very high. Secondly, we observed from the data that, during the actual spike of emission of the micro-discharge, no x-ray emission is arriving at the GEM detector from the planar anode (as seen in Figure 15). This could indicate the presence, in this time frame, of a plasma layer around the plane electrode itself, which prevents electrons from impinging directly on the plane and stops the Bremsstrahlung radiation going out of the chamber.

4 | CONCLUSIONS AND FUTURE PERSPECTIVES

In this work the analyses performed on the x-ray data collected with the GEM detector installed at HVPTF in 2022 were presented. The needle-plane electrode configuration was observed in order to have large statistics on the micro-discharge occurrence. The study was related to successive high voltage ramps corresponding to conditioning procedures for the electrodes.

The analysis of the temporal evolution of the incoming radiation was useful to identify the microscale dynamics of the emission, becoming visible below the µs sampling time, and common features were made recognisable across all the micro-discharges considered. Additionally, the capabilities of the GEM detector were exploited for a combined space-time analysis, in which the evolution of the spatial distribution of the emission was observed and the contributions of the different channels of the detector commented.

In the context of future analyses concerning HVPTF, a simulation code is under development, based on the calculation of the voltage profiles in the vacuum chamber (with different electrode configurations) and the transport of electrons in said profiles. This could help in an attempt of reproduction of the observed dynamics, in order to understand the conditions that lead to the occurrence of the various phenomena observed and develop a theory to justify them. Additionally, new experimental sessions have been set up at the facility, in order to study different electrode configurations as well (sphere-plane, for example), and a new GEM detector is under development to take the place of the previous one. The new concept has an anode with smaller pads in the middle of the active area (3×3 mm^2), in order to avoid detector saturation and to be able to analyse the micro-discharge spikes in finer detail.

ACKNOWLEDGEMENTS

This work has been carried out within the framework of the EUROfusion consortium, funded by the European Union via the Euratom Research and Training Programme (Grant Agreement No 101052200—EUROfusion). Open access

publishing facilitated by Universita degli Studi di Milano-Bicocca, as part of the Wiley - CRUI-CARE agreement.

CONFLICT OF INTEREST STATEMENT

The authors declare no conflicts of interest. Views and opinions expressed are however those of the authors only and do not necessarily reflect those of the European Union or the European Commission. Neither the European Union nor the European Commission can be held responsible for them. This work was carried out within the framework of the ITER RFX Neutral Beam Testing Facility (NBTF) Agreement and received funding from the ITER Organisation. The views and opinions expressed herein do not necessarily reflect those of the ITER Organisation. This work has been carried out in collaboration and financial support of INFN-Group 5 (Technology Research), in the framework of the PLASMA4BEAM2 experiment.

DATA AVAILABILITY STATEMENT

The data that support the findings of this study are available from the corresponding author upon reasonable request.

ORCID

Federico Caruggi https://orcid.org/0000-0002-5480-1327

REFERENCES

1. Hemsworth, R.S., et al.: Overview of the design of the ITER heating neutral beam injectors. New J. Phys. 19(2), 025005 (2017)
2. Toigo, V., et al.: The PRIMA Test Facility: SPIDER and MITICA test-beds for ITER neutral beam injectors. New J. Phys. 19(8), 085004 (2017)
3. De Lorenzi, A., et al.: HVPTF—the high voltage laboratory for the ITER neutral beam test facility. Fusion Eng. Des. 86(6), 742–745 (2011)
4. Spagnolo, S., et al.: Characterization of x-ray events for a vacuum high voltage holding experiment. In: 2020 29th International Symposium on Discharges and Electrical Insulation in Vacuum (ISDEIV), pp. 58–61. IEEE, (2021)
5. Kushoro, M.H., et al.: Characterization of vacuum HV microdischarges at HVPTF through x-ray bremsstrahlung spectroscopy. J. Instrum. 17(1), C01054 (2022)
6. Sauli, F.: The gas electron multiplier (GEM): operating principles and applications. Nucl. Instrum. Methods Phys. Res. Sect. A Accel. Spectrom. Detect. Assoc. Equip. 805, 2–24 (2016)
7. Caruggi, F., et al.: Performance of a triple GEM detector equipped with Al-GEM foils for x-rays detection. Nucl. Instrum. Methods Phys. Res. Sect. A Accel. Spectrom. Detect. Assoc. Equip. 1047, 167855 (2023)
8. Pezzotta, A., et al.: GEMINI, a CMOS 180 nm mixed-signal 16-channel ASIC for Triple-GEM detectors readout. In: 2015 IEEE SENSORS - Proceedings (2015)
9. Muraro, A., et al.: Development and characterization of a new soft x-ray diagnostic concept for tokamaks. J. Instrum. 14(8), C08012 (2019)
10. Cancelli, S., et al.: Electronic readout characterisation of a new soft x-ray diagnostic for burning plasma. J. Instrum. 17(8), C08028 (2022)
11. Cancelli, S., et al.: Characterisation of N2-GEM: a beam monitor based on Ar-N2 gas mixture. J. Instrum. 18(5), C05005 (2023)
12. Caruggi, F., et al.: Development of a Triple-GEM detector with strip readout and GEMINI chip for x rays and neutron imaging. J. Instrum. 19(2), C02015 (2024)
13. Croci, G., et al.: nGEM fast neutron detectors for beam diagnostics. Nucl. Instrum. Methods Phys. Res. Sect. A Accel. Spectrom. Detect. Assoc. Equip. 720, 144–148 (2013)
14. Muraro, A., et al.: MBGEM: a stack of borated GEM detector for high efficiency thermal neutron detection. Eur. Phys. J. Plus 136(7), 1–14 (2021)
15. Cancelli, S., et al.: Development of a ceramic double thick GEM detector for transmission measurements at the VESUVIO instrument at ISIS. J. Instrum. 16(6), P06003 (2021)
16. Pilan, N., et al.: Study of high DC voltage breakdown between stainless steel electrodes separated by long vacuum gaps. Nucl. Fusion 60(7), 076010 (2020)
17. Caruggi, F., et al.: Development of a data analysis software for the XR-GEM installed at HVPTF and preliminary results. In: 2023 30th International Symposium on Discharges and Electrical Insulation in Vacuum (ISDEIV), pp. 29–32. IEEE, (2023)
18. Spada, E., et al.: Theoretical basis and experimental validation of the breakdown induced by rupture of dielectric layer model. IEEE Trans. Plasma Sci. 47(5), 2759–2764 (2019)
19. Diamond, W.T.: A model of gas desorption and radiation during initial high voltage conditioning in vacuum. J. Appl. Phys. 126(19), 193303 (2019)

How to cite this article: Caruggi, F., et al.: Analysis of micro-discharges fine dynamics via x-ray detection on the high voltage Padova test facility experiment. High Voltage. 10(4), 1043–1052 (2025). https://doi.org/10.1049/hve2.70042